Journal of Materials Chemistry

Cite this: *J. Mater. Chem.*, 2011, **21**, 12321

www.rsc.org/materials

PAPER

Three growth modes and mechanisms for highly structure-tunable SnO_2 nanotube arrays of template-directed atomic layer deposition†

Xiangbo Meng, Yong Zhang, Shuhui Sun, Ruying Li and Xueliang Sun*

Received 9th April 2011, Accepted 25th May 2011
DOI: 10.1039/c1jm11511a

This article presents a vapor-phase strategy to synthesize highly structure-tunable SnO_2 nanotube arrays of high aspect ratio, which features atomic layer deposition of SnO_2 on anodic aluminium oxide templates using $SnCl_4$ and H_2O as precursors. This systematic study disclosed that there are three distinctive temperature-dependent growth modes, *i.e.*, layer-by-layer, layer-by-particle, and evolutionary particles contributing to the structural uniqueness of the resultant SnO_2 nanotubes. The layers were identified in an amorphous phase while the particles in a crystalline phase. As a consequence, the synthesized SnO_2 nanotubes are not only phase-controllable but also morphology-transferable with growth temperatures. In a following effort to explore the underlying mechanisms, as another contribution of this study, three growth models were proposed and clarified. Thus, this study offers not just a precise alternative for synthesizing structurally novel nanotubes but scientific insights into fundamentals as well.

1. Introduction

Nanostructured materials are nowadays providing modern societies with more and more promising solutions to our challenges faced, *e.g.*, serving as important components in alternative renewable energy sources in place of the depleting fossil fuels.[1] The main reason lies in their exceptional properties resulting from their size-dependency features. Therefore, there is an ever-increasing interest in synthesizing various nanostructures. In this context, one-dimensional (1D) nanostructures (including nanorods, nanobelts, nanowires, and nanotubes) represent one important class and have been receiving growing attention.[2] In comparison, nanotubes are benefited by their hollow structure as well as higher surface-to-volume ratios, and thereby exhibit many advantages over their solid counterparts in emerging applications. It is demonstrated that, for example, metal oxide nanotubes surpass other forms of nanomaterials including carbon nanotubes (CNTs) in sensing ability, photo catalytic activity, water photolysis efficiency, and photovoltaic behavior.[3] Thus, the development of novel nanotubular metal oxides is apparently critical for future nanodevices.

Among metal oxides, tin(IV) dioxide (SnO_2) is distinguished with a wide band gap (3.6 eV at 300 K), high optical transparency, low resistance, and high conductivity.[4] As a consequence, SnO_2 nanostructures have found their usefulness in sensors,[4,5] batteries,[6] solar cells,[7] and field emission,[8] *etc.* Under these circumstances, 1D SnO_2 nanotubes have been widely synthesized *via* various strategies, mainly falling into two categories: solution-based[9–16] and vapor-phase[17–21] methods. Despite these efforts, the previous practices were exposed to some drawbacks as well. In the cases of solution-based processes,[9–16] they consist of a series of complex procedures and are usually tedious, ranging from ten to several tens of hours. In the cases of vapor-phase methods,[17–21] they in general need high temperatures (with the lowest one reported at 800 °C[21]). Furthermore, the two methods still commonly suffer some apparent deficiency in precisely manipulating the synthesis of nanotubular SnO_2, and they exclusively produced polycrystalline SnO_2 nanotubes.

To circumvent the disadvantages suffered in the aforementioned studies, we recently explored a new route to synthesize SnO_2 nanotubes, featuring the use of atomic layer deposition (ALD) on anodic aluminium oxide (AAO, *i.e.*, Al_2O_3) templates. As is well known, ALD is a surface-controlled process relying on two alternating gas–solid reactions. Thus, it can precisely control the film deposition at the atomic level and provide unrivaled conformality and excellent uniformity.[22] In this study, we performed the synthesis of SnO_2 nanotubes by exercising the ALD of SnO_2 (ALD-SnO_2) on AAO templates. This template-directed ALD process used $SnCl_4$ and water as precursors. It is apparent that the reaction between the two precursors would produce SnO_2, as described below:

$$SnCl_4 + 2H_2O \rightarrow SnO_2 + 4HCl \quad (1)$$

In the ALD-SnO_2 processes, the sequential adsorption of the two kinds of precursor molecules (*i.e.*, $SnCl_4$ and H_2O) on the inner

Department of Mechanical and Materials Engineering, The University of Western Ontario, London, ON, Canada N6A 5B8. E-mail: xsun@eng.uwo.ca

† Electronic supplementary information (ESI) available. See DOI: 10.1039/c1jm11511a

surfaces of the AAO pores resulted in the formation of tubular SnO_2 nanostructures, *i.e.*, SnO_2 nanotubes in aligned arrays. Thus, this template-directed ALD route is advantageous over those[17–21] in literature for the fabrication of SnO_2 nanotubes. First of all, the use of AAO templates helped to produce nanotubes with aligned arrays of high aspect ratio (up to 300 : 1). More importantly, this strategy offers high tunability in manipulating the structures of as-synthesized SnO_2 nanotubes. As will be revealed, the ALD-SnO_2 on AAO contributed to the growth of SnO_2 nanotubes with three modes with increased temperatures, *i.e.*, layer-by-layer, layer-by-particle, and evolutionary particles. The layers were identified in the amorphous phase while the particles were in the crystalline phase. Thus, the resultant SnO_2 nanotubes are phase-controllable and morphology-transferable. In particular, the intriguing results ignited our great curiosity to explore the underlying mechanisms and then three growth models were proposed for their occurrences. Therefore, this study not only opened an alternative avenue for synthesizing novel SnO_2 nanotubes in a highly controllable manner, but also provided scientific insights to ALD growth. It is believed that the resultant SnO_2 nanotubes would provide multiple choices as promising components for many important applications.

2. Experimental

2.1. Template-directed ALD-SnO_2 for tubular nanostructures

ALD-SnO_2 was performed on AAO templates in a commercial ALD reactor (Savannah 100, Cambridge Nanotechnology Inc., USA). AAO templates (Whatman, Anodisc, 60 μm in thickness and 13 mm in diameter) with a nominal pore size of 200 nm were first placed in the heated reactor chamber before each ALD process. Then, tin(IV) chloride (99% $SnCl_4$, Sigma-Aldrich) and deionized water as precursors were supplied into the reactor in an alternating manner when the reactor reached a set temperature. The temperatures (T) were adjusted in the range 150–400 °C. Nitrogen served as the carrier gas with a flow rate of 20 sccm and the ALD reactor was sustained at a low level of base pressure (typically 0.4 Torr) by a vacuum pump (Pascal 2005 I, Adixon). The ALD procedures were set as follows: (1) a 0.5-s supply of $SnCl_4$; (2) a 3.0-s extended exposure of $SnCl_4$ to AAO; (3) a 10.0-s purge of oversupplied $SnCl_4$ and any by-products; (4) a 1.0-s supply of H_2O vapor; (5) a 3.0-s extended exposure of H_2O to AAO; and (6) a 10.0-s purge of oversupplied H_2O and any by-products. The aforementioned six-step sequence constituted one ALD-SnO_2 cycle and the ALD processes were changeable in their cycling numbers.

In Fig. 1, the fulfillment of the template-directed ALD strategy is schematically illustrated for the fabrication of SnO_2 nanotube arrays. Fig. 1(a) shows the ALD-SnO_2 coating on an AAO template, in which the $SnCl_4$ (A) and water (B) pulses proceeded alternatively. When the precursor molecules were penetrating AAO pores, they would chemisorb on the inner surfaces. With increased ALD-cycles, a SnO_2 covering formed on the inner walls of the nanosized pores as well as the outer surface of the AAO template (see Fig. 1(b)). As will be disclosed in this article, the covering characters changed with the ALD cycling numbers as well as growth temperatures. The outer covering of AAO was removed mechanically by fine sandpapers and then an array of SnO_2 nanotubes (see Fig. 1(c)) was exposed. A following 30-min etching of 0.5 M sodium hydroxide (NaOH) dissolved AAO and uncovered an array of separated SnO_2 nanotubes (see Fig. 1(d)). In the Fig. 1(a)–(c), the cross-sections of a few of AAO pores are to better illustrate the change induced by the ALD coating.

2.2. Characterization

The synthesized SnO_2 nanotubes were characterized using a field-emission scanning electron microscope (FE-SEM, Hitachi 4800*S*) equipped with energy dispersive X-ray spectroscopy (EDS), transmission electron microscope (TEM, Philips CM10), high-resolution TEM (HRTEM, JEOL 2010 FEG), and micro X-ray diffractometer (XRD, Brucker D8, Cu-Kα radiation, λ = 1.5406 Å).

3. Results and discussion

3.1. Results

Fig. 2 shows the XRD patterns of 1000-cycle ALD-SnO_2 on AAO at different temperatures, *i.e.*, 150, 200, 300, and 400 °C as indicated by 'a', 'b', 'c', and 'd', respectively. Fig. 2(a) discloses that there are no characteristic peaks at the growth temperature of 150 °C, implying the amorphous nature of the deposited SnO_2. In contrast, Fig. 2(b)–(d) show many characteristic peaks when the growth temperatures are higher than 200 °C, consistent with the reference values for the crystalline SnO_2 of tetragonal rutile phase (JCPDS PDF No. 41-1445). In addition, it is also noticeable that the peaks in Fig. 2(b) are much broader and less intense than the ones in both Fig. 2(c) and (d), indicating that the crystals produced at 200 °C should be much smaller. It is apparent that

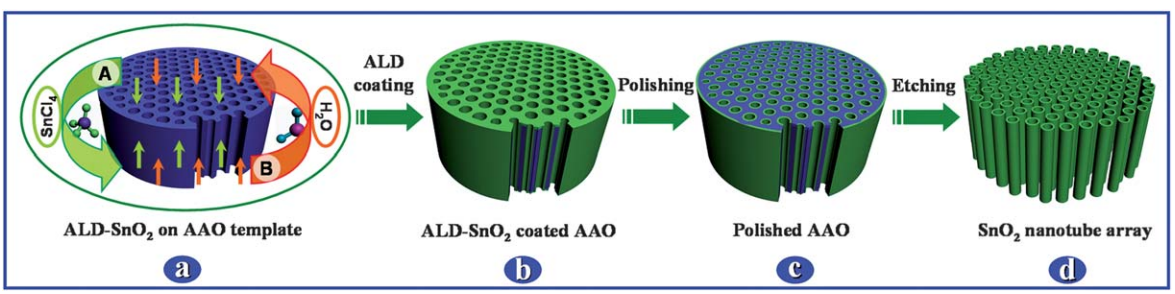

Fig. 1 Schematic fabrication of SnO_2 nanotubes *via* template-directed ALD: (a) the ALD-SnO_2 coating on an AAO template, (b) the ALD-coated AAO template, (c) the mechanically polished AAO template, and (d) the received SnO_2 nanotube array.

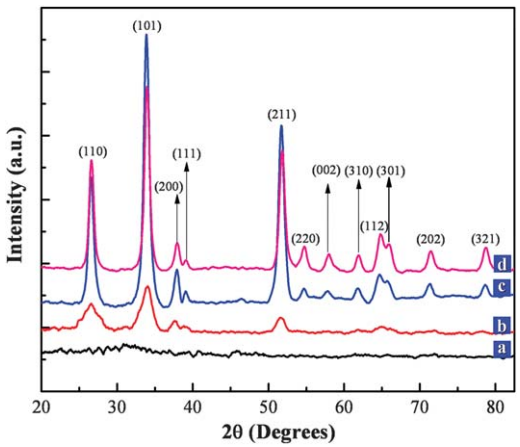

Fig. 2 XRD patterns of 1000-cycle ALD-SnO_2 at different growth temperatures: (a) 150, (b) 200, (c) 300, and (d) 400 °C.

the temperatures played important roles and induced phase-transition in ALD-SnO_2 processes. To further investigate the temperature-dependent characters of ALD-SnO_2 as well as the resultant SnO_2 nanotubes, we applied various tools such as EDS, SEM, and HRTEM, and the results will be demonstrated in the following parts.

The growth characteristics of the ALD-SnO_2 were first examined at the temperature of 150 °C, as shown Fig. 3. Fig. 3(a) shows the EDS spectrum of the ALD-SnO_2 coated AAO, and it demonstrates the presence of Sn. The Al component is attributed

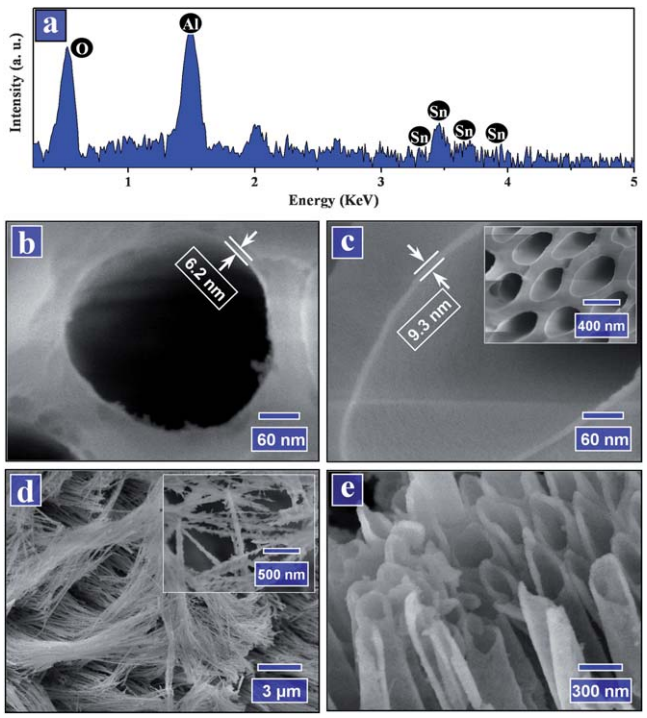

Fig. 3 The growth characteristics of ALD-SnO_2 at 150 °C: (a) EDS spectrum of the ALD-SnO_2 on AAO; top views of AAO after (b) 1000 and (c) 1500 cycles of ALD-SnO_2; the template-removed SnO_2 in the forms of (d) clusters and (e) nanotubes corresponding to 1000 and 1500 cycles, respectively.

to AAO whereas O is partially from AAO and partially from the ALD-SnO_2. Combined with the XRD pattern of Fig. 2(a), it is reasonable to conclude that amorphous SnO_2 has been deposited on AAO. To obtain the information on the ALD-SnO_2 of the AAO pores, the top views (the SEM images in Fig. 3(b) and (c)) on the polished AAO disclose that a uniform layer has been formed on their inner walls after 1000 and 1500 cycles, accounting for a deposited film of 6.2 and 9.3 nm, respectively. Thus, it is able to know that the ALD-SnO_2 at 150 °C experienced a nearly linear growth rate of 0.062 Å/cycle, accounting for a layer-by-layer growth mode. In addition, Fig. 3(c) clearly shows that the inner surface is very smooth and that the AAO pores were equally coated (the inset of Fig. 3(c)). To obtain free-standing SnO_2 nanotubes, AAO templates were etched by a 0.5 M NaOH solution. It was found that, in the case of 1000 cycles (Fig. 3(d) and inset), the nanotubes are easy to split during the etching process. As a result, the resultant pieces leaned against and formed well regulated clusters. A similar phenomenon has been previously reported in the literature.[10] In the case of 1500 cycles (Fig. 3(e)), SnO_2 nanotubes were achieved, probably due to the improved strength with the increased wall thickness. However, it is noticed that the walls of the SnO_2 nanotubes (Fig. 3(e)) become thickened to around 30 nm. The reason probably lies in their amorphous nature being vulnerable to the NaOH solution, leading to a swelling change during the etching process of AAO.

XRD patterns in Fig. 2(b)–(d) indicate that phase-transition occurred in ALD-SnO_2 processes when temperatures were increased to 200 °C or higher. To investigate the temperature-dependent effects, the ALD-SnO_2 at 200 °C was examined, as illustrated in Fig. 4. Fig. 4(a) shows the side-view images to the cross-sections of AAO pores after 500, 1000, and 1500 cycles of ALD-SnO_2. The cycling numbers are indicated on the left-bottom corners of the three images. Obviously, in each case there is a uniform layer deposited in AAO pores and the thickness is identifiable, *i.e.*, 7.0, 8.9, and 9.8 nm as marked in the images. In addition, it is worth noting that there are more and more clusters formed on the top of the layers, consisting of numerous nanoparticles of around 5 nm. In particular, the layers show a decreasing growth per cycle (GPC) while the clusters grow bigger, accounting for 0.14, 0.038, and 0.018 Å/cycle in each sequential 500 cycles. In Fig. 4(b), it is shown that the deposited SnO_2 can produce nanotube arrays when AAO was etched away. Furthermore, Fig. 4(c) shows the TEM image of a piece of debris for the deposited materials of 1500 cycles, and the selected area electron diffraction (SAED, the inset of Fig. 4(c)) patterns disclose the polycrystalline character. A higher magnification TEM image (Fig. 4(d)) on a local area (as marked by 'd' in Fig. 4 (c)) confirms that the clusters consist of numerous nanoparticles of around 5 nm, consistent with the wide XRD peaks of Fig. 2(b). Fig. 4(e) reveals the HRTEM observation on another local area in Fig. 4(c), consisting of a part of the beneath layer and a part of a cluster. It reveals that the beneath layer by nature is amorphous while the cluster is crystalline in structure. As denoted in Fig. 4 (e), the inter-plane spacing of 0.335 nm is identifiable for some nanoparticles, which is consistent with the (110) planes of rutile SnO_2 (JCPDS PDF No. 41-1445). Furthermore, the amorphous area was further examined with higher magnification, as shown in Fig. 4(f). It is disclosed that the beneath layer is arranged in

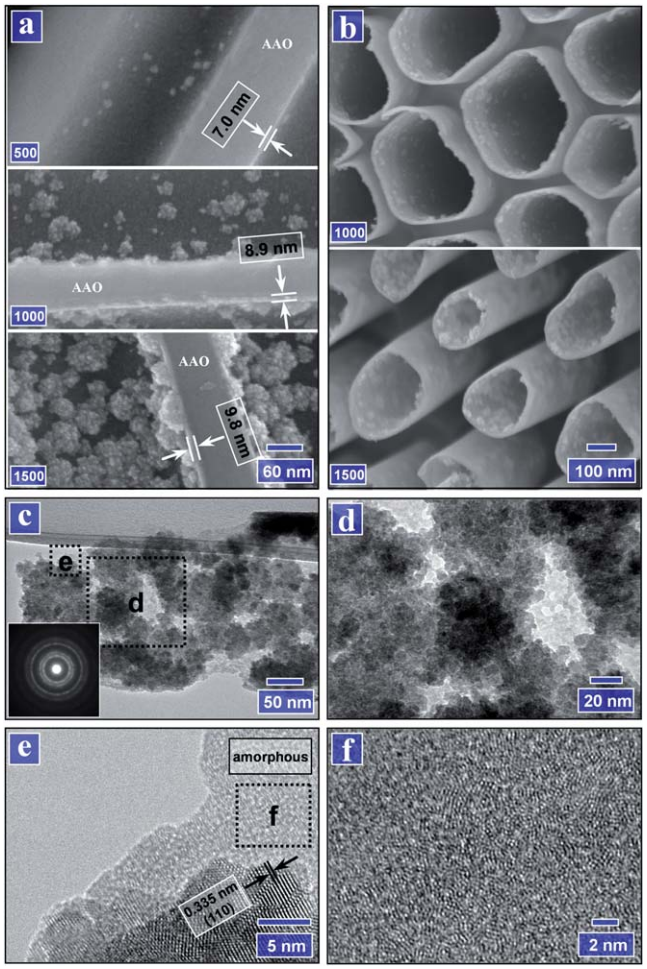

Fig. 4 The growth characteristics of ALD-SnO_2 at 200 °C: (a) SEM side views of AAO pores after 500, 1000, and 1500 cycles of ALD-SnO_2; (b) the received nanotube arrays of ALD-SnO_2 of 1000 and 1500 cycles after AAO templates were etched away; (c) TEM image for a piece of debris of the deposited SnO_2 after 1500-cycle ALD-SnO_2 (inset: SAED patterns); (d) high-magnification TEM image for a local area as indicated in (c); (e) HRTEM image for a local area as indicated in (c); and (f) HRTEM image for a local area of the beneath layer as indicated in (e).

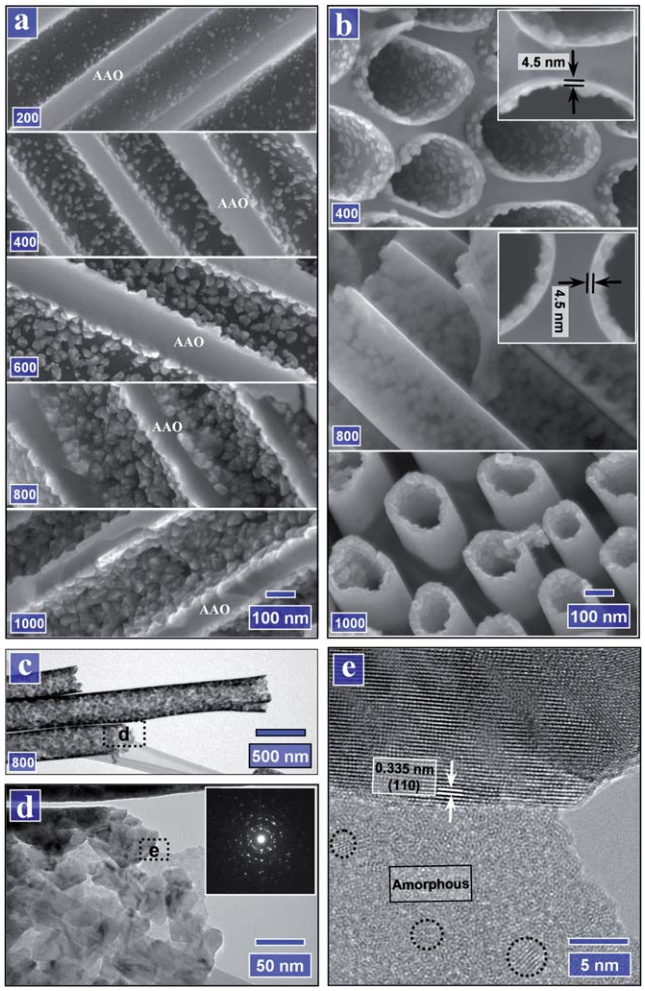

Fig. 5 The growth characteristics of ALD-SnO_2 at 300 °C: (a) SEM side views of AAO pores coated with the ALD-SnO_2 of 200, 400, 600, 800, and 1000 cycles (as marked on the left-bottom corner of each case); (b) SEM images for the received SnO_2 nanotubes after 400, 800, and 1000 ALD-cycles (insets: top-views on ALD-SnO_2 of 400 and 800 cycles); (c) the TEM image for the SnO_2 nanotubes of 800 ALD-cycles; (d) the high magnification TEM image for a part of a SnO_2 nanotube in (c) (inset: SAED patterns); (e) the HRTEM image for a local area in (d).

a disordered manner, but there are uncountable tiny nuclei of 1–2 nm formed. Obviously, the ALD-SnO_2 at 200 °C proceeded in a layer-by-cluster (or particle) growth mode, in which the growth of the amorphous layer is preferable before the clusters takes predominance. In comparison to the case of ALD-SnO_2 at 150 °C, the layer growth at 200 °C is much faster in the first 500 cycles (Fig. 4(a)) but is hindered by the increasing advent of nanoparticle clusters in the following ALD processes.

Fig. 5 illustrates the ALD-SnO_2 growth characteristics due to the increased temperature of 300 °C. Fig. 5(a) shows five SEM images of the side views of AAO pores, corresponding to the ALD-SnO_2 of 200, 400, 600, 800, and 1000 cycles in a sequence from top to bottom, respectively. The cycling number is indicated on the left-bottom corner of each image as well. It is obvious that there were more and more nanoparticles deposited in the pores while they were growing larger from 15 to 40 nm with increased cycles. In addition, it is also observable from the images that there is also a thin layer underneath the particles (see also Fig. SI-1 in the Supporting Information†). Upon 1000 cycles, it is noticeable that the growing particles have squished into each other and completely covered the inner walls. In Fig. 5(b), it is shown that the ALD-SnO_2 formed a series of nanotubes. The nanotubes are featured by smooth outer surfaces and nanoparticle-decorated inner surfaces. In particular, the nanoparticles are tunable in both size and amount by simply adjusting the ALD cycles. It is also noticed that the beneath layer is uniform with a thickness of 4.5 nm after 200 ALD-cycles and the thickness remains constant in the following ALD processes (see the insets in Fig. 5(b) as well as Fig. SI-1 in the Supporting Information†). In Fig. 5(c), the received SnO_2 nanotubes of 800 ALD-cycles are shown by a TEM image and one local area is enlarged in Fig. 5(d). The inset of Fig. 5(d) indicates the polycrystalline nature of the nanotubes by SAED patterns. Furthermore, Fig. 5(e) discloses that the particles are crystalline

while the beneath layer is amorphous. In particular, the characteristic planes of (110) are observed with some nanoparticles, showing an inter-plane distance of 0.335 nm. In addition, it is also observed that there are numerous tiny nuclei (as circled for some in Fig. 5(e)) appearing on the amorphous layer, accounting for the increased amount of crystalline particles with increased cycles. Thus, the ALD-SnO_2 at 300 °C also experienced a layer-by-particle growth mode, in which the amorphous layer grew first before the growth of the crystalline nanoparticles took the predominance. Apparently, the deposited crystalline SnO_2 nanoparticles are responsible for the XRD peaks of Fig. 2(c).

Obviously, the information from Fig. 4 and 5 jointly disclosed a layer-by-particle growth mode, where the layers are amorphous and the particles are crystalline. This novel growth mode prompted our further investigation on the effects of temperatures. As a consequence, it was also found that the layer-by-particle growth still occurred at the temperatures of 250 and 350 °C. The results for the two cases are included in Fig. SI-2 and SI-3 in the Supporting Information,† respectively. It was observed that there is an amorphous layer of 6.2 nm for ALD-SnO_2 at 250 °C, but in the case of 350 °C the layer is too thin to quantify (in spite of its observable existence). In addition, it can also be observed that crystalline particles appear much earlier and grow faster with increased temperatures, accounting for an average GPC of 0.24 and 0.3 Å/cycle for 300 and 350 °C, respectively. Thus, it is reasonable to conclude that temperatures have evident effects on the evolution of the layer-by-particle mode. In other words, the higher the temperature is, the thinner the amorphous layer can develop but the faster the crystalline particles can grow. This was also confirmed by XRD patterns of 200-cycle ALD-SnO_2 at different temperatures (see Fig. SI-4 in the Supporting Information†). There are no peaks observed for the cases of 200 and 250 °C, but peaks begin to appear at 300 °C and then become stronger and easier for identification in the cases of 350 and 400 °C. Thus, temperatures are essential for adjusting the double-layered amorphous-crystalline SnO_2 nanotubes. In return, various double-layered SnO_2 nanotubes were developed, featuring adjustable amorphous layers and crystalline particles, as shown in Fig. 4 and 5, as well as in Fig. SI-1–SI-3.†

As the temperature was increased up to 400 °C, however, the growth of ALD-SnO_2 exhibited some new characteristics, as illustrated in Fig. 6. Fig. 6(a) shows four SEM images of the side views of AAO pores, corresponding to the ALD-SnO_2 of 400, 600, 800, and 1000 cycles, respectively. The cycling number is indicated on the left-bottom corner of each image. It is clearly shown in Fig. 6(a) that the ALD-SnO_2 deposited only nanoparticles on the inner walls of AAO pores and that there is a sharp boundary between the nanoparticles and the inner surfaces. In other words, the beneath amorphous layer, as are observed in the range 200–350 °C, is unobservable at the case of 400 °C. In addition, it is noticed from Fig. 6(a) that nanoparticles stopped lateral growth but continued their growth upwards along radial orientations after 600 ALD-cycles. Correspondingly, Fig. 6(b) shows the received SnO_2 nanotubes after different cycles. It is found that the as-deposited nanotubes of 400 ALD-cycles are evidently porous and the porosity decreases with an increased number of cycles. In the case of 1000 ALD-cycles, the arrays of dense SnO_2 nanotubes are produced with an average

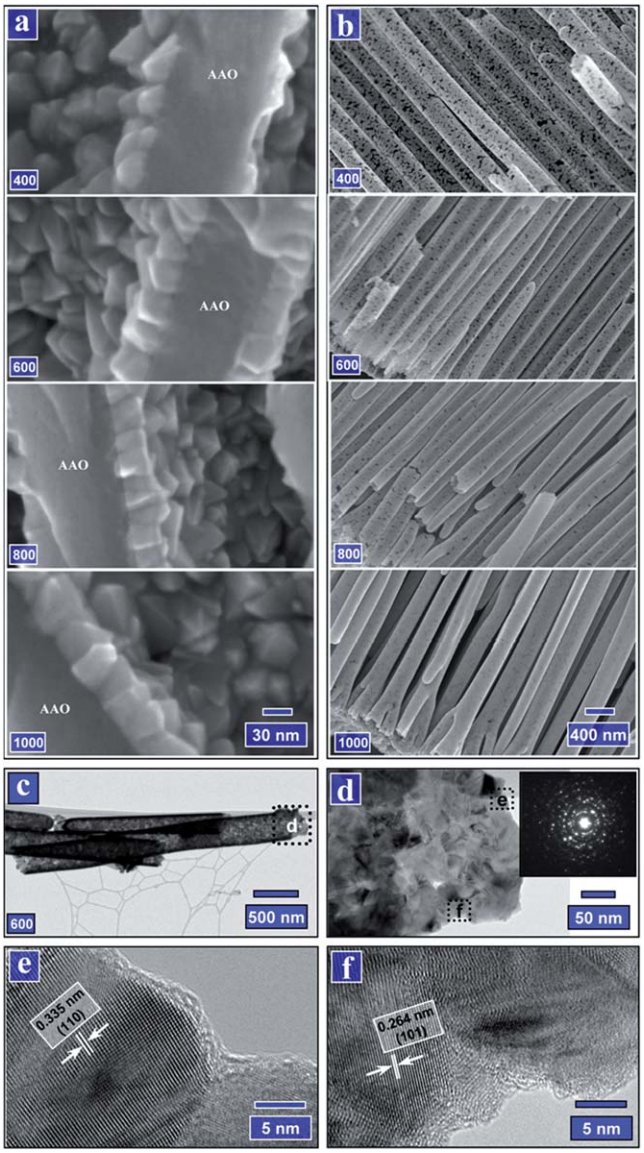

Fig. 6 The growth characteristics of ALD-SnO_2 at 400 °C: (a) SEM side views of AAO pores coated with the ALD-SnO_2 of 400, 600, 800, and 1000 cycles (as marked on the left-bottom corner of each case); (b) SEM images for the received SnO_2 nanotubes after 400, 600, 800, and 1000 ALD-cycles; (c) the TEM image for the SnO_2 nanotubes of 600 ALD-cycles; (d) the high magnification TEM image for one end of a SnO_2 nanotube in (c) (inset: SAED patterns); (e) and (f) the HRTEM images for two local areas in (d).

GPC of 0.46 Å/cycle. Obviously, the fabrication of the nanotubes at 400 °C seems a sintering process of separate nanoparticles, in which the growing nanoparticles squished each other and thereby formed nanotubes. A few of 600-cycle nanotubes were further examined with TEM, as shown in Fig. 6(c), and one end of a nanotube is enlarged in Fig. 6(d). The inset of Fig. 6(d) exposes the polycrystalline nature of the nanotubes by the SAED patterns. In addition, two local areas in Fig. 6(d) were examined with HRTEM and both commonly disclose the crystalline characteristics of nanoparticles in Fig. 6(e) and (f). Fig. 6(e) shows the characteristic planes of (110) with the inter-plane distance of 0.335 nm while Fig. 6(f) reveals the characteristic

planes of (101) with the inter-plane distance of 0.264 nm. Obviously, the ALD-SnO_2 at 400 °C is distinguishable with a growth mode of evolutionary particles.

Based on the above-disclosed results, it is remarkable that the synthesis of SnO_2 nanotube arrays by template-directed ALD revealed three temperature-dependent growth modes, *i.e.*, layer-by-layer ($T < 200$ °C), layer-by-particle ($200 \leq T < 400$ °C), and evolutionary particles ($T \geq 400$ °C), in which the layers are exclusively amorphous while the particles are commonly crystalline. In addition, it is also very apparent that the resultant nanotubes are highly structure-tunable with controllable phases and transferable morphologies. Thus, it is of great interest to explore the underlying mechanisms, especially the effects of temperatures for the intriguing results in order to gain a better understanding. On these interesting results, we will make a detailed discussion in the following sections.

3.2. Discussion

3.2.1. Effects of temperatures. In general, there are typically three key parameters in ALD processes, *i.e.*, precursors, substrates, and temperatures.[23] The three parameters combine to determine the growth characteristics of a certain material. Of the exposed precursors to date, metal chlorides and water are among the widely used pairs in ALD practice for depositing binary metal oxides. In ALD processes, substrates play two main roles: one is to shape the deposited materials in a certain form (*e.g.*, 0D, 1D, or 2D structures[24]) and the other is to initiate the deposition on their surface. A prerequisite for the latter role is that the surface of a substrate should be with reactive sites in order to chemisorb the molecules of one precursor and thereby to initiate an ALD process for a certain material. In return, the peculiarities of a substrate (*e.g.*, their structural characters as well as surface conditions) exert some influence on the growth characteristics as well as the properties of the resultant materials. However, the knowledge in this way is still very limited. With reference to temperatures, ALD requires that they should not be so high that precursors decompose, for any decomposition leads to a CVD process other than an ALD process. Even for the temperatures in the range suitable for an ALD process, it was observed that they may still result in some difference in the growth of a certain material, such as on GPC and the properties of that material.[23] Thus, growth temperatures are critical for an ALD process when its precursors and substrate are determined.

In this study, we used $SnCl_4$ and water as the precursors for the ALD-SnO_2 on AAO in order to produce nanotube arrays. Earlier studies[25–29] mainly employed them on flat substrates (*e.g.*, glass, silicon, and α-alumina) to deposit 2D thin films. Although the researchers noticed to some extent the occurrence of phase-transition with increased temperatures, the underlying mechanisms were hardly touched. It was demonstrated[29] that $SnCl_4$ and water are stable under the temperatures up to 600 °C. Thus, the temperatures of 150–400 °C in this study met the requirements of ALD processes. In particular, as revealed above, the characters of the as-synthesized nanotubes show an evident dependence on their growth temperatures in this study. Thus, it is of our great curiosity to explore the effects of temperatures as well as the underlying mechanisms. Based on reviewing earlier studies, we noticed that increased temperatures might have taken effect on the other two parameters, *i.e.*, AAO and the precursors, and thereby result in different growth behaviors, consequently leading to the highly structure-tunable nanotubes. Thus, the effects of increased temperatures deserve a special discussion, as detailed below.

(A) On AAO template. As stated above, the surface nature of a substrate is crucial for ALD processes and it should be reactive to at least one precursor. In this study, the amorphous AAO template was used as the substrate for synthesizing SnO_2 nanotubes. Thus, its surface, especially the characters and coverage of reactive sites on the inner surfaces of AAO pores, is critical for the initiation and the subsequent growth of ALD-SnO_2. Previous studies revealed that, no matter what the fabrication method was, AAO is commonly covered by hydroxyl groups as well as water molecules.[30–32] There are many types of hydroxyl groups identified, such as isolated and hydrogen-bonded ones.[30,33–38] Correspondingly, it was also experimentally[30,33–35] and theoretically[36–38] demonstrated that all types of hydroxyl groups as well as oxygen bridges are among the candidate groups to react with metal chlorides. In addition, a recent study showed that water coverage of a surface also has an important influence on surface reactions in ALD processes.[38]

With increased temperatures, it was observed that the substrate surface generally experiences some change. It was previously demonstrated that, for example, the hydrogen-bonded hydroxyl groups and water coverage decrease in amount with increased temperatures, resulting in the isolated hydroxyl groups available as principal bonding sites.[30,32,33,35,38] A mechanism for the decrease of hydrogen-bonded hydroxyl groups is the dehydroxylation of adjacent hydroxyl groups:[39]

$$2\|\text{–OH} \rightarrow \|\text{=O} + H_2O(g) \quad (2)$$

where the symbol $\|$ denotes the substrate surface and (g) refers to gas phase species. As a consequence, this dehyroxylation causes the appearance of oxygen bridges on the surface while it reduces the number of hydroxyl groups. Thus, increased temperatures tend to change the functional groups (either types or amounts, or the both) on the substrate surface.

(B) On surface reactions. Besides the influences on the surface conditions of AAO templates, increased temperatures are also inclined to affect ALD processes as well. As is well-known, as a surface-controlled process, ALD proceeds *via* two alternating self-saturating surface reactions and each precursor induces a half-reaction. Thus, increased temperatures can take effect on the precursors by changing their corresponding surface reactions and thereby result in different growth characteristics. In the case of the ALD-SnO_2, there are two surface reactions suggested previously:[40]

$$\|\text{–OH} + SnCl_4(g) \rightarrow \|\text{–O–}SnCl_3 + HCl(g) \quad (3\text{-A})$$

$$\|\text{–Cl} + H_2O(g) \rightarrow \|\text{–OH} + HCl(g) \quad (3\text{-B})$$

The half-reaction (reaction 3-A) due to a pulse of $SnCl_4$ and the half-reaction (reaction 3-B) due to a pulse of H_2O consist of one typical 'A–B' cycle to deposit SnO_2 in the ALD-SnO_2 process. As

a result, the 'A–B' cycling builds up SnO_2 films in AAO pores. Apparently, this surface chemistry is applicable to explain the growth of the amorphous layers in Fig. 3–5. However, it is evidently insufficient to address the growth of the nanoparticles (clusters) in Fig. 4–6, for it betrayed the layer-by-layer nature of ALD processes. Thus, increased temperatures might have changed one or both of the aforementioned surface reactions in reaction 3-A and reaction 3-B, and thereby led to other mechanisms. To address this issue, other researchers conducted lots of inspiring work, though the answer has not been fixed to date due to its complicated nature.

The growth of crystalline particles, in addition to the cases discussed in this study, was also observed in the ALD processes of TiO_2[41] and ZrO_2[33] when growth temperatures are higher than 300 °C. In particular, the aforementioned studies commonly used metal chlorides and water as precursors. Many experimental efforts[30,34,35] were dedicated to investigate the behind stories and proposed various mechanisms. Unfortunately, none of the mechanisms could account for the experimental observations of crystalline particle formation. Also unsuccessful were the efforts from simulations.[36–38] This kind of phenomenon is so intriguing that Puurunen[42] made a special review which attempted to provide a comprehensive explanation. Based on the examinations on earlier studies, Puurunen claimed that ligand exchange (as shown in reactions 3-A and 3-B) is the most prevalent mechanism for amorphization at low temperature (<300 °C) whereas a prominent two-step chlorination in the pulses of metal chlorides underlies the growth of crystalline particles at high temperature (>300 °C). In particular, the two mechanisms compete for dominance with temperatures. Thus, there are two different rules for ALD processes of using metal chlorides and water as precursors, and their predominance is determined by temperatures. Thanks to Puurunen's contributions, it becomes possible to explicate the growth of crystalline particles and amorphous layers. In the case of ALD-SnO_2 of using $SnCl_4$ and water, the following reactions might be induced in the pulses of $SnCl_4$ when temperatures were increased:[43,44]

$$\|\text{–OH} + SnCl_4(g) \rightarrow \|\text{–Cl} + Sn(OH)Cl_3(g) \quad (4\text{-A1})$$

$$\|\text{–OH} + Sn(OH)Cl_3(g) \rightarrow \|\text{–Cl} + Sn(OH)_2Cl_2(g) \quad (4\text{-A2})$$

$$2\|\text{–Cl} + Sn(OH)_2Cl_2(g) \rightarrow \|\text{–O}_2\text{–}SnCl_2 + 2HCl(g) \quad (4\text{-A3})$$

$$\|\text{–O}_2\text{–}SnCl_2 + Sn(OH)_2Cl_2(g) \rightarrow \|\text{–}(SnO_2)_2Cl_2 + 2HCl(g) \rightarrow \cdots \rightarrow \|\text{–}(SnO_2)_nCl_2 + 2HCl(g) \quad (4\text{-A4})$$

In the above reactions, $SnCl_4$ first chlorinates the surface hydroxyl groups and forms an intermediate hydroxychloride molecule ($Sn(OH)_2Cl_2$) by two steps, as shown in reactions 4-A1 and 4-A2. Then the hydroxychloride reacts with the surface chlorine groups through its hydroxyl groups, as shown in reaction 4-A3. In particular, the chlorine groups on the right side of the former reaction 4-A3 might further react with hydroxychloride and result in a chain of reactions, as shown in reaction 4-A4. Thus, surface reactions in the pulses of $SnCl_4$ could contribute to formation of a multilayer under high temperatures. As a consequence, nanoparticles could grow more quickly at high temperatures than at low temperatures after a same number of ALD cycles, for high temperatures should be more favorable for reaction 4-A4. This is consistent with our results, as disclosed in Fig. 4–6 as well as in Fig. SI-1–SI-3 in Supporting Information.† In addition, the above reactions also provide the answers for the size-varied nanoparticles and the continuously newly-appeared nanoparticles on the inner surfaces of the AAO pores, for some sites might be involved in a chain of reactions (as shown in reaction 4-A4) whilst others might not. With reference to the reaction happening in the pulses of water, it was suggested[42] to be still ligand exchange, as shown in the following reaction 4-B:

$$\|\text{–Cl} + H_2O(g) \rightarrow \|\text{–OH} + HCl(g) \quad (4\text{-B})$$

To summarize the above discussion, it is clear that there are two different mechanisms for the growth of amorphous layers and crystalline particles. In particular, the two compete for dominance with increased temperatures. Previous studies[30,33–35,41] observed the particle growth when the temperature is higher than 300 °C. However, as clearly demonstrated in this study, crystalline particles appeared to grow when the temperatures reached 200 °C or higher. This is likely due to lower cycles studied by previous studies, for they mainly worked on the first several cycles. As a whole, the three growth modes appearing in our work provide evidence for the two mechanisms.

Obviously, the above discussion is exclusively based on hydroxyl groups. As stated before, increased temperatures may reduce hydrogen-bonded hydroxyl groups and induce more oxygen bridges. Thus, it is necessary to address their effects on ALD-SnO_2. In contrast to a general acceptance on the roles of hydroxyl groups, there is a debate on the effects of oxygen bridges, as detailed by Puurunen.[42] Some earlier studies[33,41] suggested that metal chlorides can attack oxygen bridges *via* dissociation. However, some later studies[34,35] questioned its validity and Puurunen[42] even excluded the possibility for oxygen bridges to participate in the growth of crystalline particles. Recent simulations[36–38] suggested that oxygen bridges are possible to react with metal precursors. However, their reaction rates are much lower than those for hydroxyl groups[37] while their adsorption energy and reaction opportunity highly depend on the water coverage.[38] Remarkably, the issue on oxygen bridges is far from giving a clearly defined answer in this work and it deserves further investigation in the future. Even so, we would still suggest the reaction between $SnCl_4$ and oxygen bridges as follows, based on previous studies:[33,36–39,41]

$$\|\text{=O} + SnCl_4(g) \rightarrow \|\text{–Cl} + \|\text{–O–}SnCl_3 \quad (5)$$

Apparently, the above reaction chlorinates oxygen bridges *via* a cleavage. In a following interaction between water and the produced chlorine groups, the resultant reactions are still *via* ligand exchange,[36–38] similar to those stated in reaction 3-B or 4-B, and they create new hydroxyl groups. Thus, oxygen bridges may contribute to the growth of crystalline particles with increasing ALD cycles at elevated temperatures as well, for the created hydroxyl groups can also initiate reactions as stated in reactions 4-A1–4-A4.

3.2.2. Three growth models. In the above section, it was discussed that temperatures could influence the growth of ALD-SnO_2 by changing the surface nature of AAO as well as surface reactions of ALD processes. In terms of surface chemistry, it is disclosed that there are different mechanisms for the growth of amorphous layers and crystalline particles, which can explain our results well. Based on the aforementioned discussion and in order to better illustrate the three growth modes revealed in our study, we schematically demonstrate them with three models in Fig. 7.

Fig. 7(a) provides the model for layer-by-layer growth. As is disclosed above, this growth is predominant at low temperatures (<200 °C, see Fig. 3). In this case, the surface of the AAO pores suffers less change in its reactive sites. Consequently, abundant hydroxyl groups as well as possible high water coverage are preferable for $SnCl_4$ to interact with multiple adsorption sites.[38] The ALD-SnO_2 initiates on the AAO surface by ligand exchange, as described in reactions 3-A and 3-B. In the following $SnCl_4$ and water pulses, ligand exchange proceeds and contributes a layer-by-layer growth. As illustrated by Fig. 7(a1)–(a4) in side views of AAO pores, increased ALD-cycles contribute to the increase in film thickness. In this case, the GPC (as disclosed in Fig. 3) is pretty low, for surface reactivity is very limited under low temperatures. Fig. 7(a5) shows a resultant SnO_2 nanotube with a well-controlled amorphous wall.

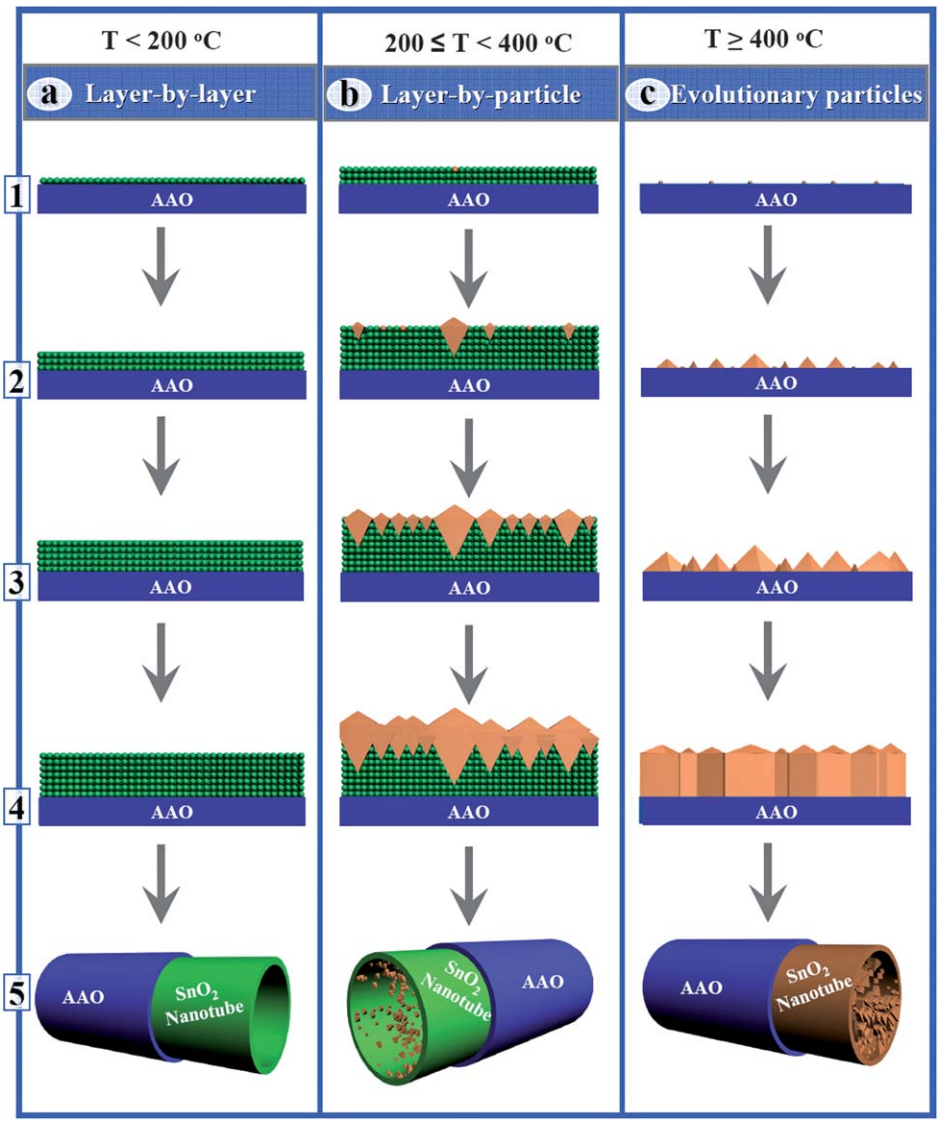

Fig. 7 Three growth models for ALD-SnO_2 nanotube arrays. At a temperature lower than 200 °C, the ALD-SnO_2 was built up in AAO pores in a mode of (a) layer-by-layer growth, as schematically shown in (a1–4) with uniform films of increasing thickness; in the range 200–400 °C, the ALD-SnO_2 experienced a mode of (b) layer-by-particle growth: (b1) amorphous layers prevailed at the initial stage but random nucleation happened with increased films, (b2) crystals grew laterally and radially while new nuclei appeared with increased films, (b3) crystals saturated on the surface and amorphous layers stopped growing, (b4) crystals stopped their lateral growth and competed with each other for their radial growth; at a temperature no less than 400 °C, the ALD-SnO_2 transferred to a mode of (c) evolutionary particle: (c1) nuclei formed immediately on the substrate surface at the starting of the ALD process, (c2) crystals grew quickly with increased ALD-cycles, (c3) crystals saturated on the substrate surface, (c4) crystals grew predominantly in their radial direction. In (a5), (b5), and (c5), the produced nanotubes were schematically illustrated.

Fig. 7(b) illustrates the layer-by-particle growth in the temperature range 200–400 °C. In this temperature range, results (see Fig. 4, 5, as well as Fig. SI-1–SI-3 in the Supporting Information†) revealed that the dominant growth changes from amorphous layers to crystalline particles. It was also disclosed that the ultimate thickness of amorphous layers is constant for a certain temperature and decreases with increased temperatures. Contrary to the reducing layers, however, the particles grow faster with temperatures. The mechanisms lie in the competing effects between ligand exchange and chlorination, *i.e.*, lower temperatures are favorable for ligand exchange while higher temperatures prompt chlorination.[42] In this kind of growth, the AAO surface nature is exposed to a higher possibility for change, depending on the adopted temperature. Meanwhile, increased temperatures may also improve surface reactivity and induce some reactions which do not occur at lower temperatures.[23] As illustrated by Fig. 7(b1), a side view on AAO pores shows that amorphous layers take the priority to deposit, probably due to the favorable surface nature of AAO and its amorphous structure. With increasing layers, however, nucleation events (illustrated by orange dots) happen randomly on the layers and the layers may be also favorable for the growth of nuclei, for they have a different nature with respect to AAO. Further increased ALD-cycles, as illustrated in Fig. 7(b2), prompt the crystals to grow in both lateral and radial directions. At the same time, more nucleation events take place while the amorphous layers grow thicker. To a certain point, as illustrated in Fig. 7(b3), the growing crystals and newborn nuclei saturate the growing surface. Since then, as illustrated in Fig. 7(b4), the amorphous layers stop growing and only crystalline particles compete for available space in the AAO pores. In the competitive growth of crystalline particles, they stop the growth in a lateral direction while continuing growth along the radial direction. As a result, the double-layered amorphous–crystalline SnO_2 nanotubes (see Fig. 7(b5)) are produced. In particular, this type of nanotube is highly tunable in structure, for the layers and particles are controllable with temperature.

Fig. 7(c) illustrates the third growth mode, evolutionary particle, under a temperature of no less than 400 °C. In this case, the AAO surface may be modified to a large extent, resulting in a considerable reduction of hydroxyl groups and water coverage but an increase of oxygen bridges. In particular, at high temperatures chlorination becomes the only mechanism for ALD-SnO_2. As a result, the modified surface conditions of AAO and the unique chlorination may combine to lead to the exclusive growth mode of crystalline particles. Fig. 7(c1) shows in a side view on the AAO pores that nuclei appear right at the beginning of the ALD-SnO_2. With increased ALD-cycles (see Fig. 7(c2)), the nuclei grow into crystals and more nuclei appear at the same time. While the nuclei crystallize, the crystals grow in both lateral and radial directions. To a certain point, the AAO surface is saturated with crystals and nuclei (see Fig. 7(c3)). Since then, the crystals begin a competitive process in which they fight each other for available space. The surviving crystals obtain the opportunities to grow only in a radial orientation. Similar competitive processes were studied in other areas where they are named as evolutionary selection.[45,46] The resultant crystalline SnO_2 nanotube is shown in Fig. 7(c5).

In summary, three temperature-dependent growth modes (*i.e.*, layer-by-layer, layer-by-particle, and evolutionary particles) were revealed for the synthesis of SnO_2 nanotubes by the template-directed ALD strategy, leading to a series of highly structure-tunable SnO_2 nanotubes. Aiming at exploring the underlying mechanisms, a detailed discussion on the effects of temperatures was conducted. It is believed that two different mechanisms of surface chemistry are responsible for the growth of amorphous layers and crystalline particles, respectively, and that the two compete for dominance with temperature. To further demonstrate the transformations of different growth modes, three growth models were proposed and schematically demonstrated. Thus, this work is helpful not only for manipulating the fabrication of novel SnO_2 nanotubes but also for scientific insights.

4. Conclusions

This work presented a template-directed ALD strategy to synthesize SnO_2 nanotubes. Using $SnCl_4$ and water as precursors, the fulfillment of ALD-SnO_2 on an AAO template revealed that this strategy features its capabilities in highly tuning the synthesized SnO_2 nanotubes. It was disclosed that the growth of SnO_2 nanotubes takes three different modes, *i.e.*, layer-by-layer, layer-by-particle, and evolutionary particles, in which the layers are amorphous while the particles are crystalline. Thus, this strategy can precisely control both phases and morphologies of the SnO_2 nanotube by simply adjusting the temperature. These intriguing results prompted our exploration on the underlying mechanisms and, based on reviewing earlier studies, the effects of temperatures were discussed. In particular, two different principles were clarified for the occurrence of amorphous layers and crystalline particles during the growth of SnO_2 nanotubes. Furthermore, three growth models were suggested to illustrate the evolutions between different growth modes with temperature. Thus, this work would be important for manipulating the synthesis of SnO_2 nanotubes and it is also helpful to meet scientific curiosities with insightful views. In addition, it is believed that the synthesized SnO_2 nanotubes would be promising as components in many applications, such as batteries, sensors, solar cells, and field emission, *etc*.

Acknowledgements

This research was supported by the Natural Science and Engineering Research Council of Canada (NSERC), Canada Research Chair (CRC) Program, Canadian Foundation for Innovation (CFI), Ontario Research Fund (ORF), Early Researcher Award (ERA) and the University of Western Ontario.

References

1 A. S. Aricò, P. Bruce, B. Scrosati, J. M. Tarascon and W. V. Schalkwijk, *Nat. Mater.*, 2005, **4**, 366–377.
2 J. Weber, R. Singhal, S. Zekri and A. Kumar, *Int. Mater. Rev.*, 2008, **53**, 235–255.
3 M. Lee, T. W. Kim, C. Bae, H. Shin and J. Kim, *JOM*, 2010, **62**, 44–49.
4 M. Batzill and U. Diebold, *Prog. Surf. Sci.*, 2005, **79**, 47–154.
5 M. Batzill, *Sensors*, 2006, **6**, 1345–1366.

6 D. Deng, M. G. Kim, J. Y. Lee and J. Cho, *Energy Environ. Sci.*, 2009, **2**, 818–837.
7 H. J. Snaith and C. Ducati, *Nano Lett.*, 2010, **10**, 1259–1265.
8 J. H. He, T. H. Wu, C. L. Hsin, K. M. Li, L. J. Chen, Y. L. Chueh, L. J. Chou and Z. L. Wang, *Small*, 2006, **2**, 116–120.
9 Y. Wang, J. Y. Lee and H. C. Zeng, *Chem. Mater.*, 2005, **17**, 3899–3903.
10 W. Zhu, W. Wang, H. Xu and J. Shi, *Mater. Chem. Phys.*, 2006, **99**, 127–130.
11 M. Lai, J. A. Gonzalez Martinez, M. Grätzel and D. J. Riley, *J. Mater. Chem.*, 2006, **16**, 2843–2845.
12 M. Lai, J. H. Lim, S. Mubeen, Y. Rheem, A. Mulchandani, M. A. Deshusses and N. V. Myung, *Nanotechnology*, 2009, **20**, 185602.
13 G. X. Wang, J. S. Park, M. S. Park and X. L. Gou, *Sens. Actuators, B*, 2008, **131**, 313–317.
14 Y. Wang, M. Wu, Z. Jiao and J. Y. Lee, *Nanotechnology*, 2009, **20**, 345704.
15 N. Wang, X. Cao and L. Guo, *J. Phys. Chem. C*, 2008, **112**, 12616–12622.
16 S. L. Chou, J. Z. Wang, H. K. Liu and S. X. Dou, *Electrochem. Commun.*, 2009, **11**, 242–246.
17 Z. R. Dai, J. L. Gole, J. D. Stout and Z. L. Wang, *J. Phys. Chem. B*, 2002, **106**, 1274–1279.
18 Y. Liu and M. Liu, *Adv. Funct. Mater.*, 2005, **15**, 57–62.
19 J. Duan, Q. Cao, S. Yang, H. Huang, X. Zhao, R. Zhang and G. Cheng, *J. Cryst. Growth*, 2006, **289**, 164–167.
20 M. Salehi, B. Janfeshan and S. K. Sadrnezhaad, *Appl. Phys. A*, 2009, **97**, 361–364.
21 Z. Li, H. Wang, P. Liu, B. Zhao and Y. Zhang, *Appl. Surf. Sci.*, 2009, **255**, 4470–4473.
22 S. M. George, *Chem. Rev.*, 2010, **110**, 111–131.
23 R. L. Puurunen, *J. Appl. Phys.*, 2005, **97**, 121301.
24 M. Knez, K. Nielsch and L. Niinistö, *Adv. Mater.*, 2007, **19**, 3425–3438.
25 A. Rosental, A. Tarre, A. Gerst, T. Uustare and V. Sammelselg, *Sens. Actuators, B*, 2001, **77**, 297–300.
26 A. Tarre, A. Rosental, V. Sammelselg and T. Uustare, *Appl. Surf. Sci.*, 2001, **175–176**, 111–116.
27 T. Takeuchi, K. Shoji, T. Tadano, I. Doteshita and S. Onodera, *Thin Solid Films*, 2003, **442**, 98–101.
28 T. Takeuchi, I. Doteshita and S. Asami, *Surf. Interface Anal.*, 2004, **36**, 1133–1135.
29 J. Lu, J. Sundqvist, M. Ottosson, A. Tarre, A. Rosental, J. Aarik and A. Harsta, *J. Cryst. Growth*, 2004, **260**, 191–200.
30 A. Kytökivi and M. Lindblad, *J. Chem. Soc., Faraday Trans.*, 1995, **91**, 941–948.
31 J. W. Diggle, T. C. Downie and C. W. Goulding, *Chem. Rev.*, 1969, **69**, 365–405.
32 G. D. Parfitt, *Pure Appl. Chem.*, 1976, **48**, 415–418.
33 A. Kytökivi, E.-L. Lakomaa and A. Root, *Langmuir*, 1996, **12**, 4395–4403.
34 S. Haukka, E.-L. Lakomaa, O. Jylhä, J. Vilhunen and S. Hornytzkyj, *Langmuir*, 1993, **9**, 3497–3506.
35 S. Haukka, E.-L. Lakomaa and A. Root, *J. Phys. Chem.*, 1993, **97**, 5085–5094.
36 Z. Hu and C. H. Turner, *J. Phys. Chem. B*, 2006, **110**, 8337–8347.
37 Z. Hu and C. H. Turner, *J. Am. Chem. Soc.*, 2007, **129**, 3863–3878.
38 A. B. Mukhopadhyay, C. B. Musgrave and J. F. Sanz, *J. Am. Chem. Soc.*, 2008, **130**, 11996–12006.
39 J. Aarik, A. Aidla, V. Sammelselg, H. Siimon and T. Uustare, *J. Cryst. Growth*, 1996, **169**, 496–502.
40 X. Du, Y. Du and S. M. George, *J. Vac. Sci. Technol., A*, 2005, **23**, 581–588.
41 M. Ritala, M. Leskelä, E. Nykänen, P. Soininen and L. Niinistö, *Thin Solid Films*, 1993, **225**, 288–295.
42 R. L. Puurunen, *Chem. Vap. Deposition*, 2005, **11**, 79–90.
43 X. Meng, D. Geng, J. Liu, M. N. Banis, Y. Zhang, R. Li and X. Sun, *J. Phys. Chem. C*, 2010, **114**, 18330–18337.
44 X. Meng, Y. Zhong, Y. Sun, M. N. Banis, R. Li and X. Sun, *Carbon*, 2011, **49**, 1133–1144.
45 A. van der Drift, *Philips. Res. Repts.*, 1967, **22**, 267–288.
46 A. B. Rodriguez-Navarro, *Thin Solid Films*, 2001, **389**, 288–295.

